

Article

# Influence of Heat Treatment on Microstructures and Mechanical Properties of NiCuCrMoTiAlNb Nickel-Based Alloy

Shuyong Jiang <sup>1,\*</sup>, Dong Sun <sup>2</sup>, Yanqiu Zhang <sup>1</sup> and Bingyao Yan <sup>2</sup>

<sup>1</sup> College of Mechanical and Electrical Engineering, Harbin Engineering University, Harbin 150001, China; zhangyq@hrbeu.edu.cn

<sup>2</sup> College of Materials Science and Chemical Engineering, Harbin Engineering University, Harbin 150001, China; 18845143035@163.com (D.S.); yaozl@hrbeu.edu.cn (B.Y.)

\* Correspondence: jiangshuyong@hrbeu.edu.cn; Tel.: +86-451-8251-9710

Received: 18 January 2018; Accepted: 20 March 2018; Published: 27 March 2018



**Abstract:** As-cast NiCuCrMoTiAlNb nickel-based alloys were subjected to two-stage heat treatment, including solution treatment and subsequent aging treatment. Furthermore, the influence of heat treatment on microstructures and mechanical properties of NiCuCrMoTiAlNb nickel-based alloys was further investigated. The as-cast NiCuCrMoTiAlNb Ni-based alloys are able to experience large plastic deformation at room temperature, where nanocrystalline phases are induced. In the case of heat-treated NiCuCrMoTiAlNb nickel-based alloys, with increasing Nb content, plenty of Ni<sub>3</sub>(Al, Ti) precipitates ( $\gamma'$  phases) are distributed in the  $\gamma$  matrix and they are able to become the obstacles to impede the movement of dislocations, which is responsible for increasing the yield strength of NiCuCrMoTiAlNb nickel-based alloys. Pile-up of dislocations in the vicinity of  $\gamma'$  precipitates adversely influences plasticity of NiCuCrMoTiAlNb nickel-based alloys.

**Keywords:** nickel-based alloy; heat treatment; plastic deformation; microstructures; mechanical properties

## 1. Introduction

Nickel-based superalloys possess high strength, creep resistance, fatigue resistance, and oxidation resistance at elevated temperatures, so they are widely employed in the aerospace industry, where several typical applications deal with gas turbines, jet engines, and so on [1–5]. In addition, some nickel-based superalloys, such as Inconel 718 [6–9], Inconel X-750 [10–12], and Hastelloy C276 [13], which are frequently employed at elevated temperatures, also become a promising candidate for manufacturing a workpiece at cryogenic temperatures because of their high structure stability, excellent ductility, high toughness, high corrosion resistance, and especially high elastic limit under cryogenic environments. Heat treatment significantly influences the microstructures of nickel-based superalloys, which further affect the corresponding mechanical properties [14–17]. In the recent literature, some researchers have reported that appropriate heat treatment modes can be used for enhancing strength [18,19], increasing hardness [20], and improving creep strength [21]. It can be generally accepted that the ability of appropriate heat treatment to enhance the mechanical properties of Ni-based alloys results from precipitation of intermetallic phases. As for most of the heat-resistant nickel-based superalloys, appropriate heat treatment is able to result in the precipitation of intermetallic phases, including gamma prime ( $\gamma'$ ), gamma double prime ( $\gamma''$ ), or delta ( $\delta$ ) [20,22]. In general,  $\gamma'$  phase, whose chemical composition is based on Ni<sub>3</sub>(Al,Ti), possesses a face-centered cubic (FCC) structure, and the chemical composition of both  $\gamma''$  and  $\delta$  phases is based on Ni<sub>3</sub>Nb, where  $\gamma''$  phase belongs to the body-centered tetragonal (BCT) structure, but  $\delta$  phase possesses an orthorhombic

structure [23,24]. Souza et al. found that  $\gamma'$  phase precipitation due to aging results in an additional increase in mechanical strength and hardness of nickel-based superalloys [25]. Li et al. stated that the smaller size of  $\gamma'$  phases, which precipitated after heat treatment, is beneficial for enhancing the Vickers hardness as well as the tensile strength of the DZ483 Ni-based superalloy [26].  $\gamma''$  phase is also the major strengthening phase of nickel-based superalloys, but it is so thermodynamically metastable that it is easy to be transformed into the more thermodynamically stable  $\delta$  phase [27]. It seems that  $\delta$  phase does not play a predominant role in strengthening nickel-based superalloys. Mignanelli et al. found that flow softening of the V207M nickel-based superalloy is closely related to the orientation of  $\delta$  phase [28]. Wen et al. stated that in the case of an appropriate initial aging time,  $\delta$  phase is capable of stimulating the occurrence of dynamic recrystallization and further improving the hot formability [29]. According to the aforementioned literature, it can be concluded that  $\gamma'$  precipitates help to enhance the mechanical properties of nickel-based superalloys at elevated temperatures, which are dependent upon the volume fraction, size, shape, and distribution of  $\gamma'$  phase. Therefore, it is of great significance to study the effect of heat treatment on the microstructures as well as the mechanical properties of nickel-based alloys so as to obtain the optimal combination of volume fraction, size, shape, and distribution of  $\gamma'$  phase [30].

In the present work, based on a new NiCuCrMoTiAlNb nickel-based alloy, the effect of heat treatment on the microstructures and mechanical properties of NiCuCrMoTiAlNb nickel-based alloy was investigated in order to improve its mechanical properties, where  $\gamma'$  phase plays an important role.

## 2. Materials and Methods

Three nickel-based alloys were fabricated and their compositions are based on Ni<sub>57-x</sub>Cu<sub>20</sub>Cr<sub>15</sub>Mo<sub>5</sub>Ti<sub>2</sub>Al<sub>1</sub>Nb<sub>x</sub> (wt %), where  $x$  represents 1, 3, and 5, respectively. In the subsequent text, the three nickel-based alloys are briefly expressed as Ni-Nb1, Ni-Nb3, and Ni-Nb5, respectively. The three nickel-based alloys were melted via the vacuum arc melting method and subsequently were made into a cylinder, which possessed a diameter of 10 mm and a length of 80 mm. Subsequently, the three as-cast nickel-based alloys were subjected to the different heat-treatment regimes. The Ni-Nb1 sample was held for 10 h at 950 °C and subsequently was quenched into water at room temperature. Then, the Ni-Nb1 sample was held for 6 h at 600 °C followed by air cooling. The Ni-Nb3 and Ni-Nb5 samples were held for 2.5 h at 1100 °C and then were quenched into water at room temperature. Subsequently, the Ni-Nb3 and Ni-Nb5 samples were held for 6 h at 650 °C followed by air cooling.

The nickel-based alloy samples with a diameter of 4 mm and a height of 6mm were cut from the as-cast and heat-treated nickel-based alloy cylinders via electro-discharge machining (EDM) (DK7725, Jiangsu Dongqing CNC Machine Tool Co., Ltd., Taizhou, China) to be employed for compression tests, which were performed on the INSTRON-5500R equipment at a strain rate of 0.001 s<sup>-1</sup> and at room temperature.

Microstructures of the three as-cast and heat-treated nickel-based alloy samples were observed using an optical microscope (OM) as well as a scanning electron microscope (SEM). In addition, microstructures of the as-cast and heat-treated Ni-Nb5 alloy samples as well as the corresponding compressed ones were also observed through a transmission electron microscope (TEM).

The samples for the OM and SEM experiments were etched in a solution whose composition is HF:HNO<sub>3</sub>:H<sub>2</sub>O = 1:2:10. Subsequently, the OM experiment was implemented via an OLYMPUS311 optical microscope (Olympus Corporation, Tokyo, Japan) and the SEM experiment was conducted via an FEI Quanta 200 SEM (University of South Carolina, Columbia, SC, USA). The composition of heat-treated nickel-based alloy samples was characterized via energy dispersive spectroscopy (EDS). The phase structure was characterized by X-ray diffraction (XRD) based on an X-ray diffractometer (Royal Dutch Philips Electronics Ltd., Amsterdam, The Netherlands). Foil samples for the TEM experiment were mechanically ground to 50  $\mu$ m and subsequently thinned by twin-jet polishing in an

electrolyte containing 6%  $\text{HClO}_4$ , 34%  $\text{C}_4\text{H}_{10}\text{O}$ , and 60%  $\text{CH}_3\text{OH}$ . An FEI TECNAI G2 F30 microscope (FEI Corporation, Hillsboro, OR, USA) was used for the TEM observations.

### 3. Results and Discussion

#### 3.1. Optical Microstructure of As-Cast Nickel-Based Alloys

Figure 1 illustrates optical micrographs of as-cast nickel-based alloys, which include Ni-Nb1, Ni-Nb3, and Ni-Nb5, respectively. It is observed from Figure 1 that the microstructures of the three nickel-based alloys consist of dendrites. In general, the dendrite grows up from the outer wall of the cylinder to the centre of the cylinder. This phenomenon means that there exists a certain non-equilibrium crystallization during solidification of nickel-based alloys.

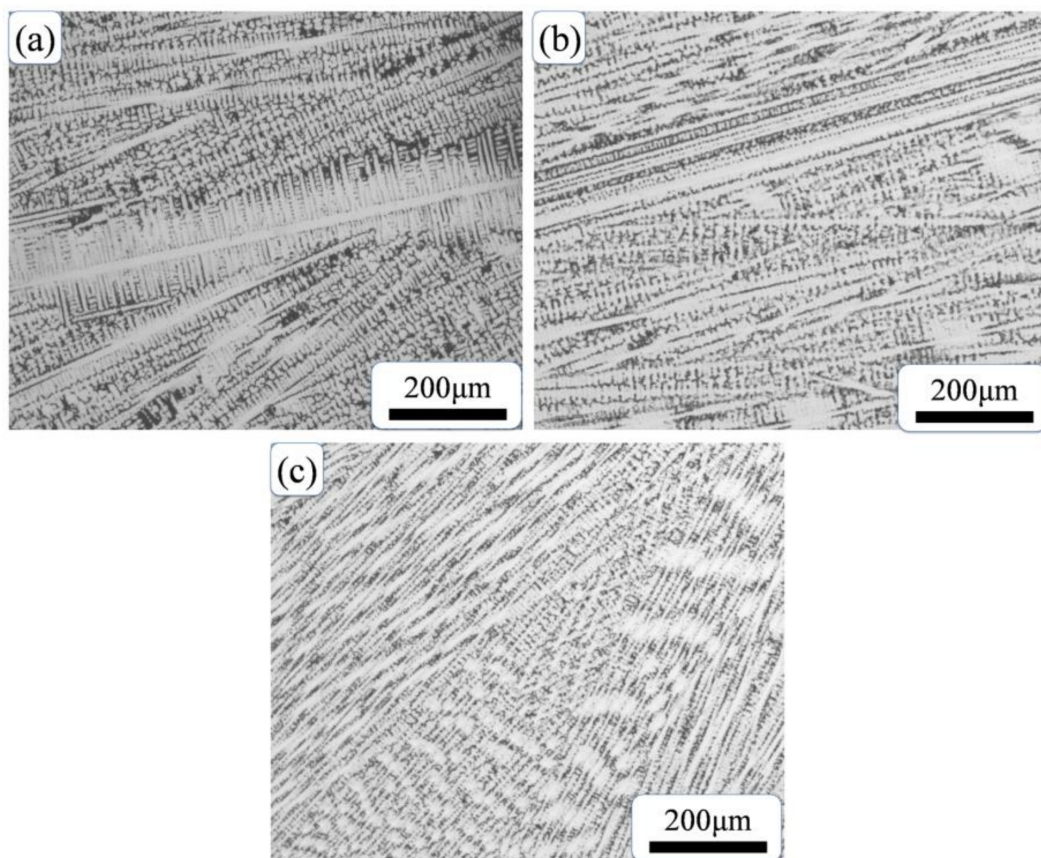


**Figure 1.** Optical micrographs of as-cast nickel-based alloys: (a) Ni-Nb1; (b) Ni-Nb3; (c) Ni-Nb5.

#### 3.2. Optical Microstructure of Heat-Treated Nickel-Based Alloys

Figure 2 illustrates metallographic micrographs of the three heat-treated nickel-based alloys. It can be observed from Figure 2 that as for the Ni-Nb1 sample, the branches of the dendrite are weakened, but the trunks of the dendrite exhibit little change. This phenomenon indicates that heat treatment has not had too much influence on the dendrite structure, which is attributed to the lower solution temperature. However, as for the Ni-Nb3 and Ni-Nb5 samples, heat treatment leads to the complete disappearance of the dendrites. Instead, the corresponding microstructures are composed of dominant column grains and a few equiaxed grains. Compared to the Ni-Nb3 sample, the Ni-Nb5 sample exhibits a smaller grain size, which means that increasing Nb content contributes to refining the microstructures.

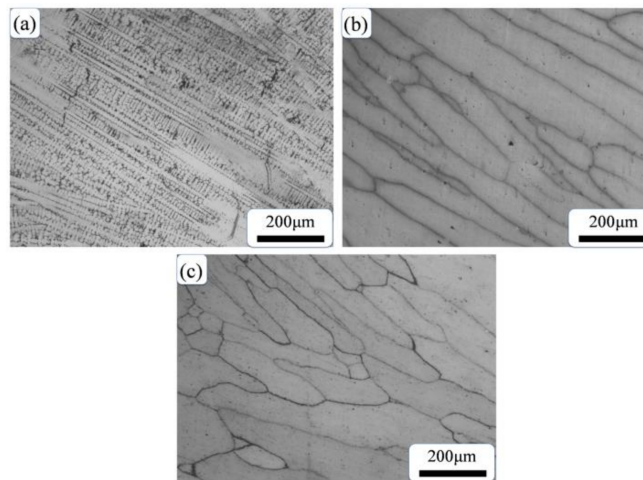


Figure 2. Optical micrographs of heat-treated nickel-based alloys: (a) Ni-Nb1; (b) Ni-Nb3; (c) Ni-Nb5.

3.3. SEM and EDS Analysis of Heat-Treated Nickel-Based Alloys

Figures 3–5 show SEM micrographs as well as the involved EDS maps of heat-treated nickel-based alloys. It can be found from Figure 3 that as for the Ni-Nb1 sample, the dendrite does not disappear completely after being subjected to heat treatment, but the composition segregation has been slightly improved. As for the Ni-Nb3 and Ni-Nb5 alloy samples undergoing heat treatment, the dendrite is completely transformed into column grains and equiaxed grains, where the redistribution of alloy elements by means of diffusion makes a contribution to reducing the composition segregation. However, it can be found from EDS maps that there still exists a certain composition variation between the grain interior and the grain boundary. In particular, for the Ni-Nb5 alloy specimen, a lot of precipitates are dispersedly embedded in the matrix.

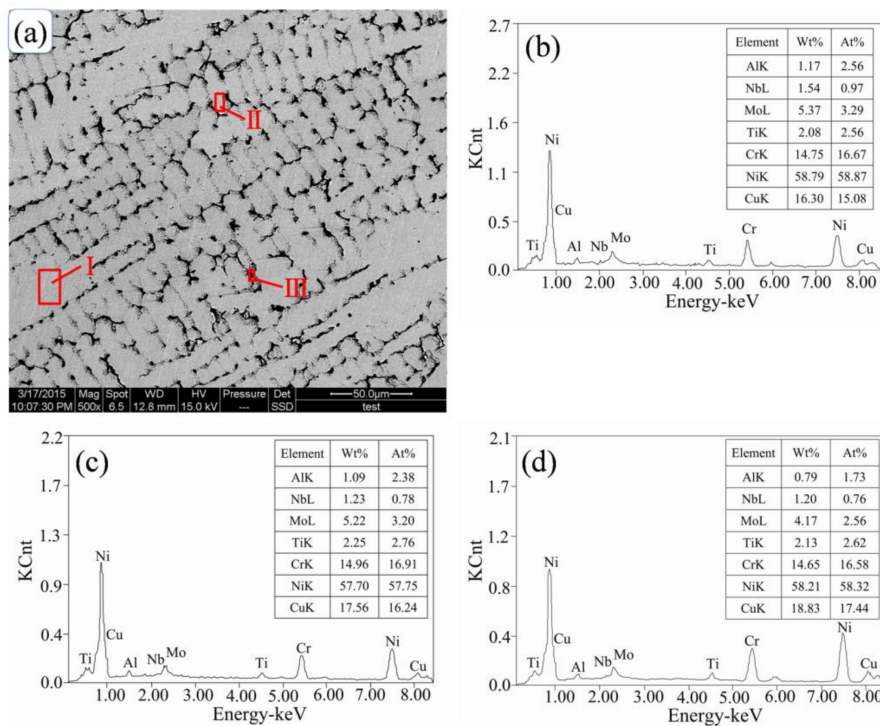
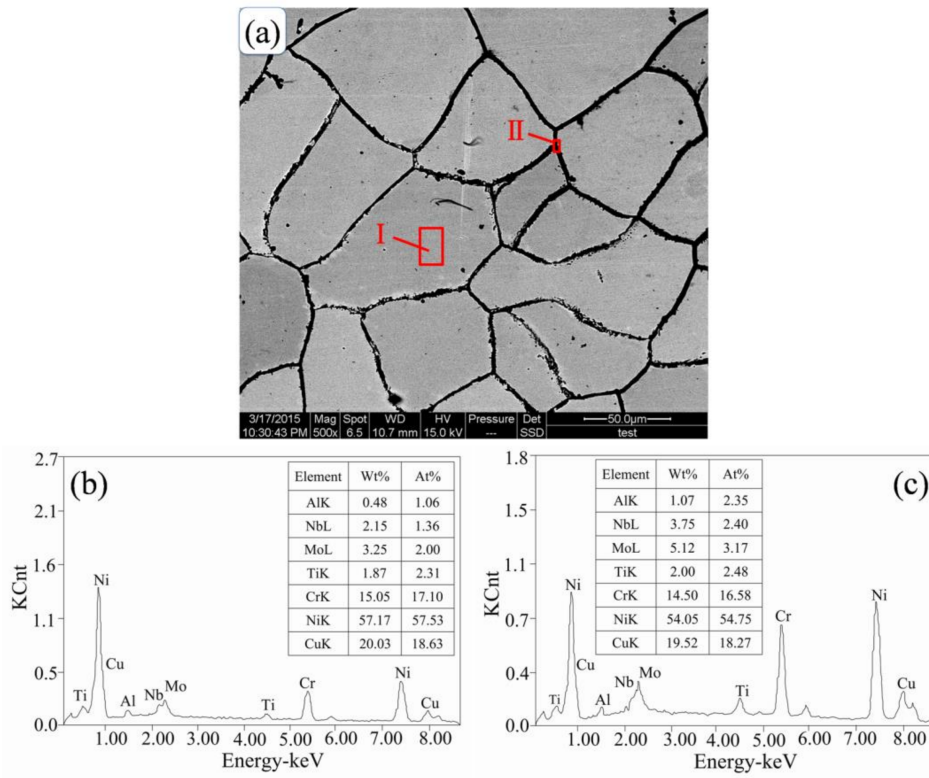
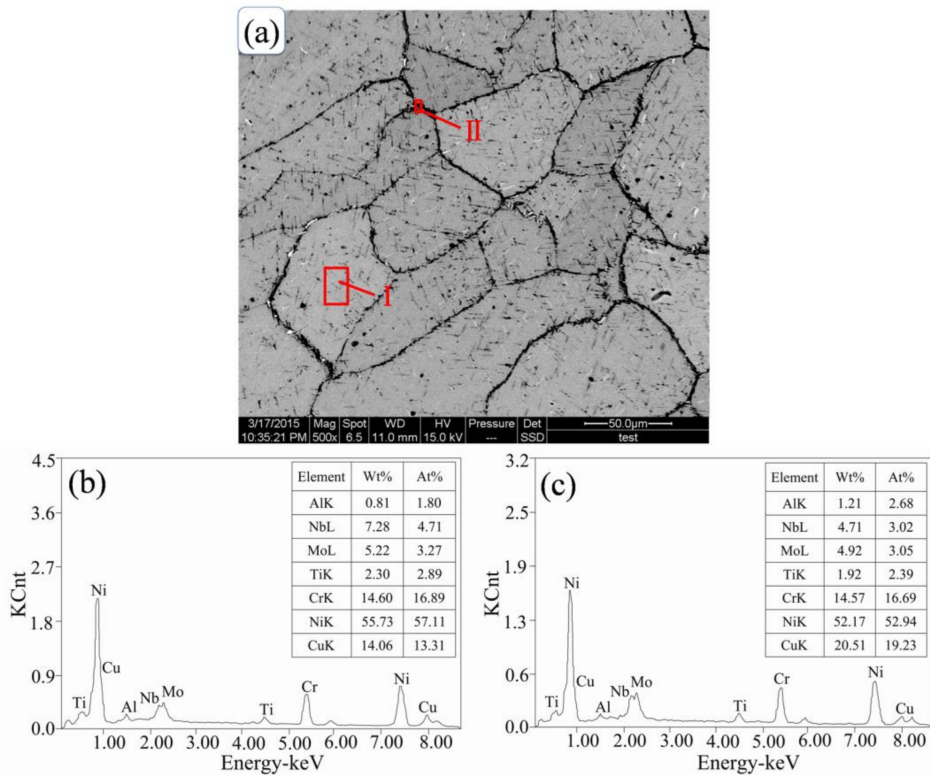


Figure 3. SEM micrographs of heat-treated Ni-Nb1 alloy along with EDS maps: (a) SEM micrograph; (b) EDS map of zone I in (a); (c) EDS map of zone II in (a); (d) EDS map of zone III in (a).



**Figure 4.** SEM micrographs of heat-treated Ni-Nb<sub>3</sub> alloy along with EDS maps: (a) SEM micrograph; (b) EDS map of zone I in (a); (c) EDS map of zone II in (a).



**Figure 5.** SEM micrographs of heat-treated Ni-Nb<sub>5</sub> alloy along with EDS maps: (a) SEM micrograph; (b) EDS map of zone I in (a); (c) EDS map of zone II in (a).

### 3.4. XRD Analysis of Heat-Treated Nickel-Based Alloys

Figure 6 illustrates XRD maps of the heat-treated nickel-based alloys. It can be found from Figure 6 that each of the three nickel-based alloys is composed of  $\gamma$ -Ni solid solution and  $\text{Ni}_3(\text{Al,Ti})$  phase ( $\gamma'$  phase). According to the XRD maps, it can be further confirmed that the precipitates illustrated in Figure 5c are  $\gamma'$  phases since no other precipitates are observed. In general, the precipitation of  $\gamma'$  phase is closely related to the heat-treatment regime. Ha et al. found that  $\gamma'$  phase can precipitate during aging at the temperature range of 620–732 °C, where the size and the volume fraction of  $\gamma'$  phase increase with increasing aging temperature [31].

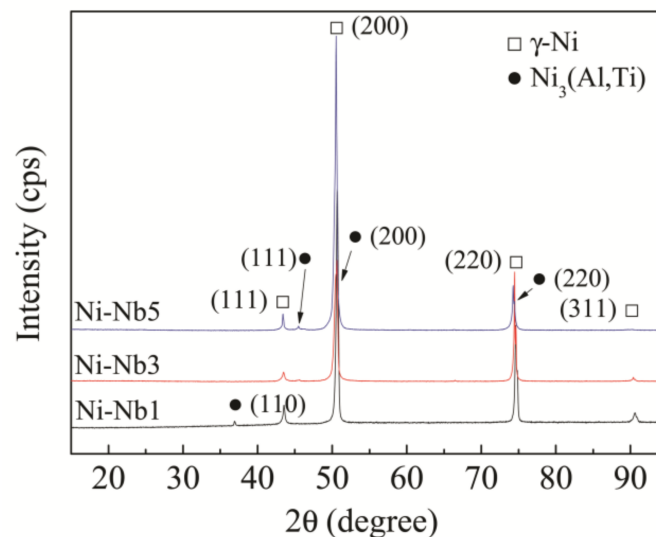
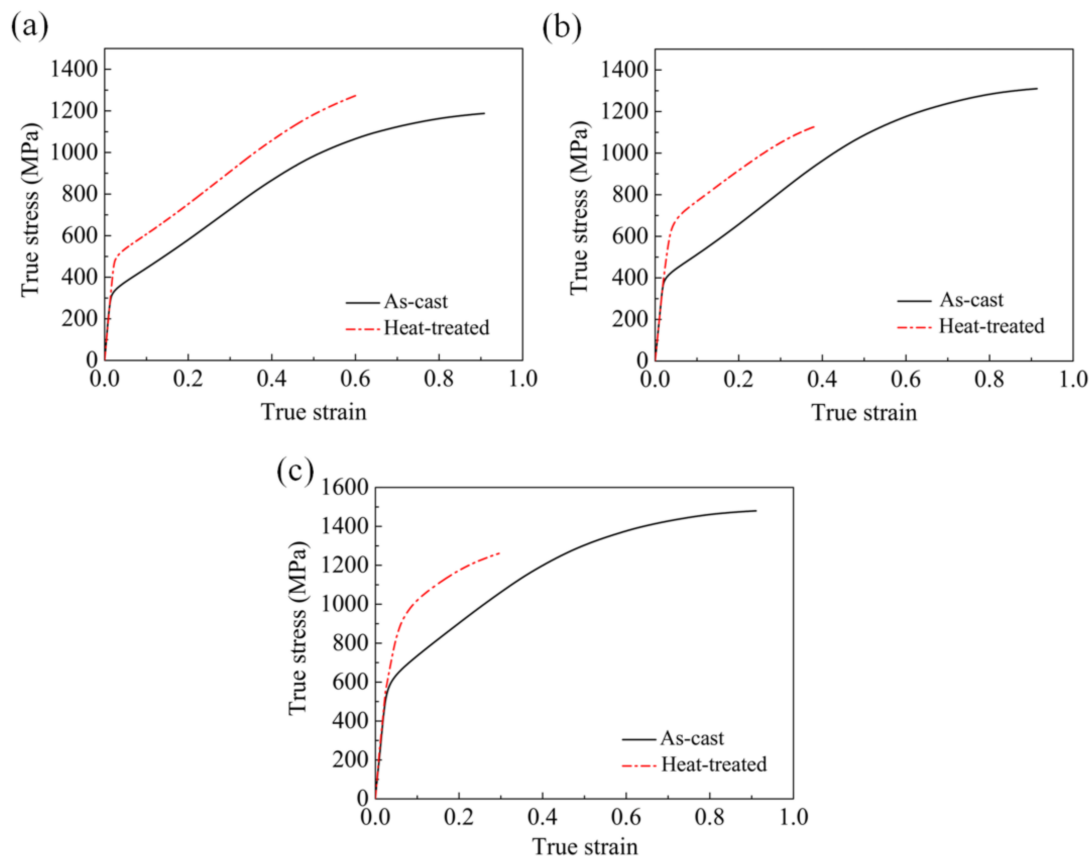


Figure 6. XRD maps of nickel-based alloys subjected to heat treatment.

### 3.5. Mechanical Properties of Nickel-Based Alloys

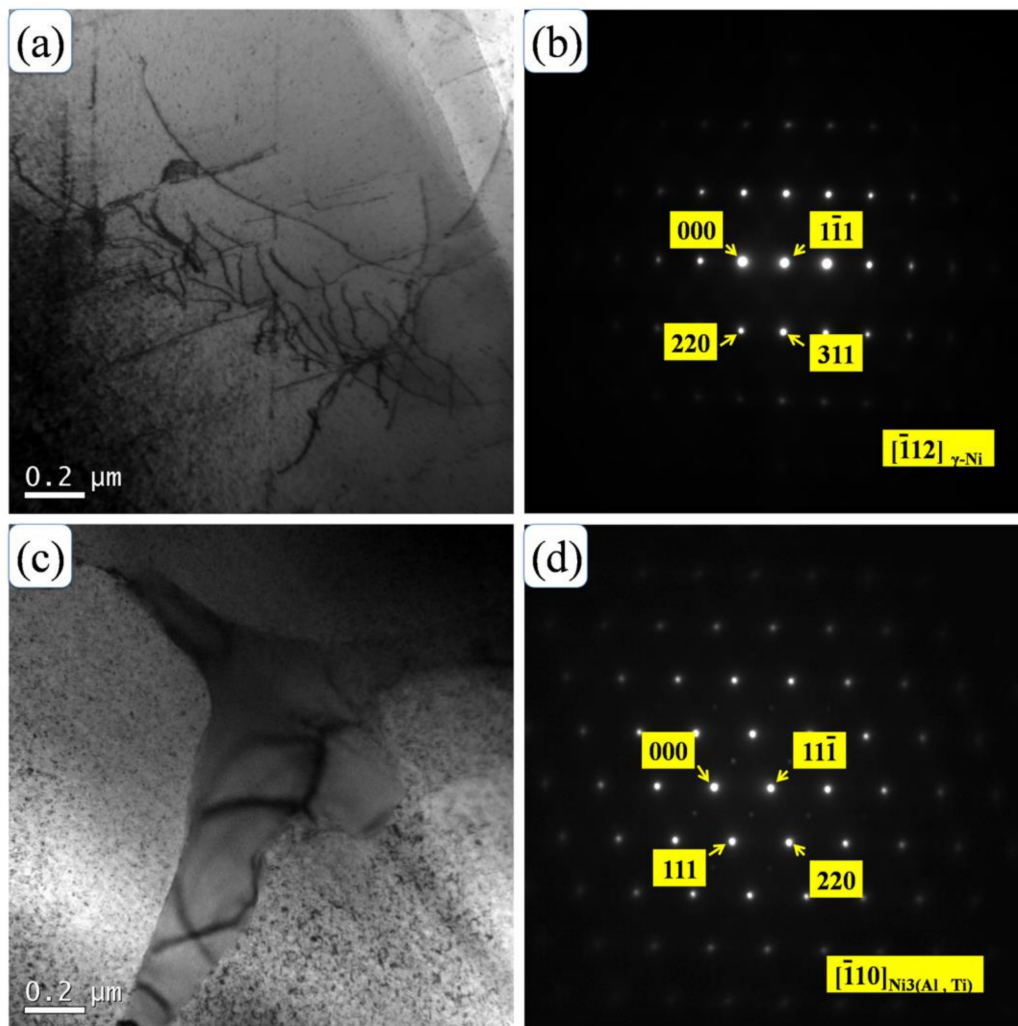
Figure 7 illustrates compressive stress-strain curves of the as-cast and heat-treated nickel-based alloys. It can be found from Figure 7 that as for the three nickel-based alloys, heat treatment contributes to enhancing the yield strength, but it leads to a decrease in the compressive strength and the plasticity. Furthermore, with increasing Nb content, yield strength is enhanced more and more substantially. The increase of yield strength is attributed to the precipitation strengthening mechanism, where  $\gamma'$  phases precipitate in the matrix and they become the obstacles to prevent the dislocations from moving. In general,  $\gamma'$  precipitate is coherently embedded in the  $\gamma$  matrix of nickel-based alloys, so the interface characteristic between  $\gamma'$  phase and  $\gamma$  matrix considerably influences the mechanical properties of nickel-based alloys [30]. Pröbstle et al. stated that the high lattice misfit at the interface between  $\gamma'$  phase and  $\gamma$  matrix can lead to dense dislocation networks, which contribute to enhancing the strength of nickel-based alloys [21]. It can be observed from Figure 5 that the Ni-Nb5 sample possesses the most  $\gamma'$  phases after being subjected to heat treatment. As a consequence, the heat-treated Ni-Nb5 sample exhibits the highest yield strength, which means that the dispersed  $\gamma'$  phases play a more advantageous role in strengthening nickel-based alloy. Increasing the Nb content helps to stabilize  $\gamma'$  phase [28]. However, there generally exists a certain contradiction between yield strength and plasticity, where the yield strength is raised and simultaneously the plasticity is lowered. The interaction between dislocations, such as dislocation pileup and dislocation tangle, can make it more difficult to activate the dislocation slip, which consequently leads to the sacrifice of the plasticity.



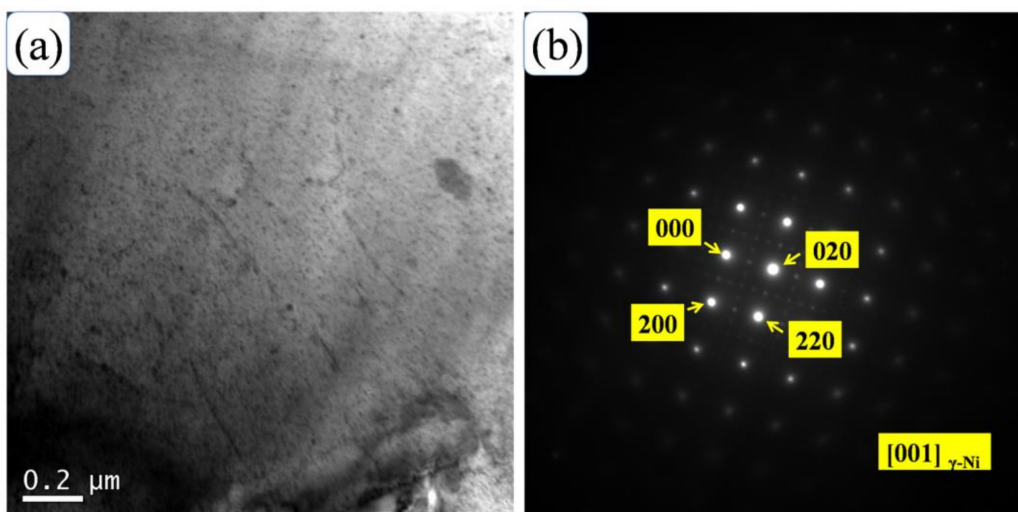
**Figure 7.** Influence of heat treatment on compressive stress-strain curves of nickel-based alloys: (a) Ni-Nb1; (b) Ni-Nb3; (c) Ni-Nb5.

### 3.6. Plastic Deformation Mechanism of As-Cast and Heat-Treated Ni-Nb5 Samples

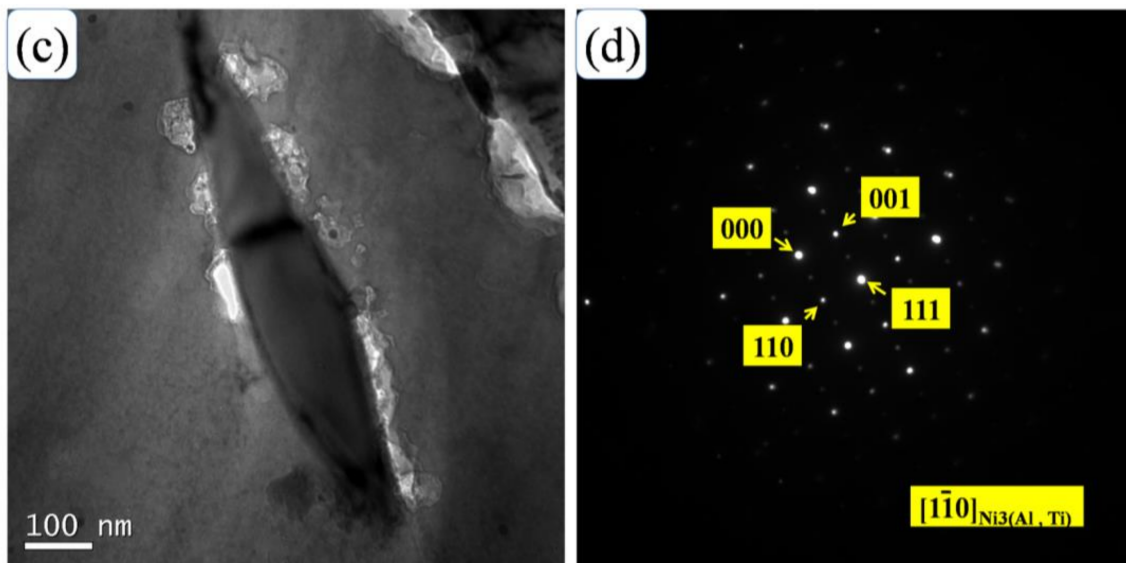
Based on the above results, it is noted that the Ni-Nb5 alloy possesses the highest yield strength. In the present work, the plastic deformation mechanisms of Ni-Nb5 alloy are further investigated based on TEM observation. Figure 8 shows TEM micrographs of the as-cast Ni-Nb5 alloy. It is observed from Figure 8 that  $\gamma$ -Ni phase is dominant in the matrix of the as-cast Ni-Nb5 sample, where an extremely small amount of  $\gamma'$  phases can be observed and exhibit a very complicated shape. Zhang et al. stated that  $\gamma'$  precipitates are also observed in the as-cast nickel-based single crystal superalloy [32]. However,  $\gamma$ -Ni phase remains dominant in the matrix of the heat-treated Ni-Nb5 alloy, and plenty of  $\gamma'$  phases are distributed in the matrix as shown in Figure 9. It can be concluded that solution treatment for 2.5 h at 1100 °C and subsequent aging treatment for 6 h at 650 °C contribute to the uniform precipitation of  $\gamma'$  phases. In particular, as compared to the as-cast Ni-Nb5 alloy,  $\gamma'$  phases show a regular needle-like shape. In general, the morphology of  $\gamma'$  phase is complicated and diverse, and it is closely associated with the heat-treatment regime. Qiu et al. stated that in a hot isostatical pressed nickel-based alloy, solution treatment below the solvus of  $\gamma'$  phase leads to the formation of finer secondary  $\gamma'$  phase with a cuboidal shape as well as a medium-size tertiary with a spherical shape [19]. Qiu et al. found that during aging heat treatment of the DZ483 nickel-based superalloy, most of the  $\gamma'$  phases exhibit a typical cuboidal shape in the dendrite core, whereas some of the  $\gamma'$  phases show a butterfly shape in the interdendritic zone [26].



**Figure 8.** TEM micrographs of the as-cast Ni-Nb5 alloy: (a) Bright field image indicating dislocations in the matrix; (b) Diffraction pattern of  $\gamma$  matrix in (a); (c) Bright field image indicating  $\text{Ni}_3(\text{Al,Ti})$  phase in the matrix; (d) Diffraction pattern of  $\text{Ni}_3(\text{Al,Ti})$  phase in (c).



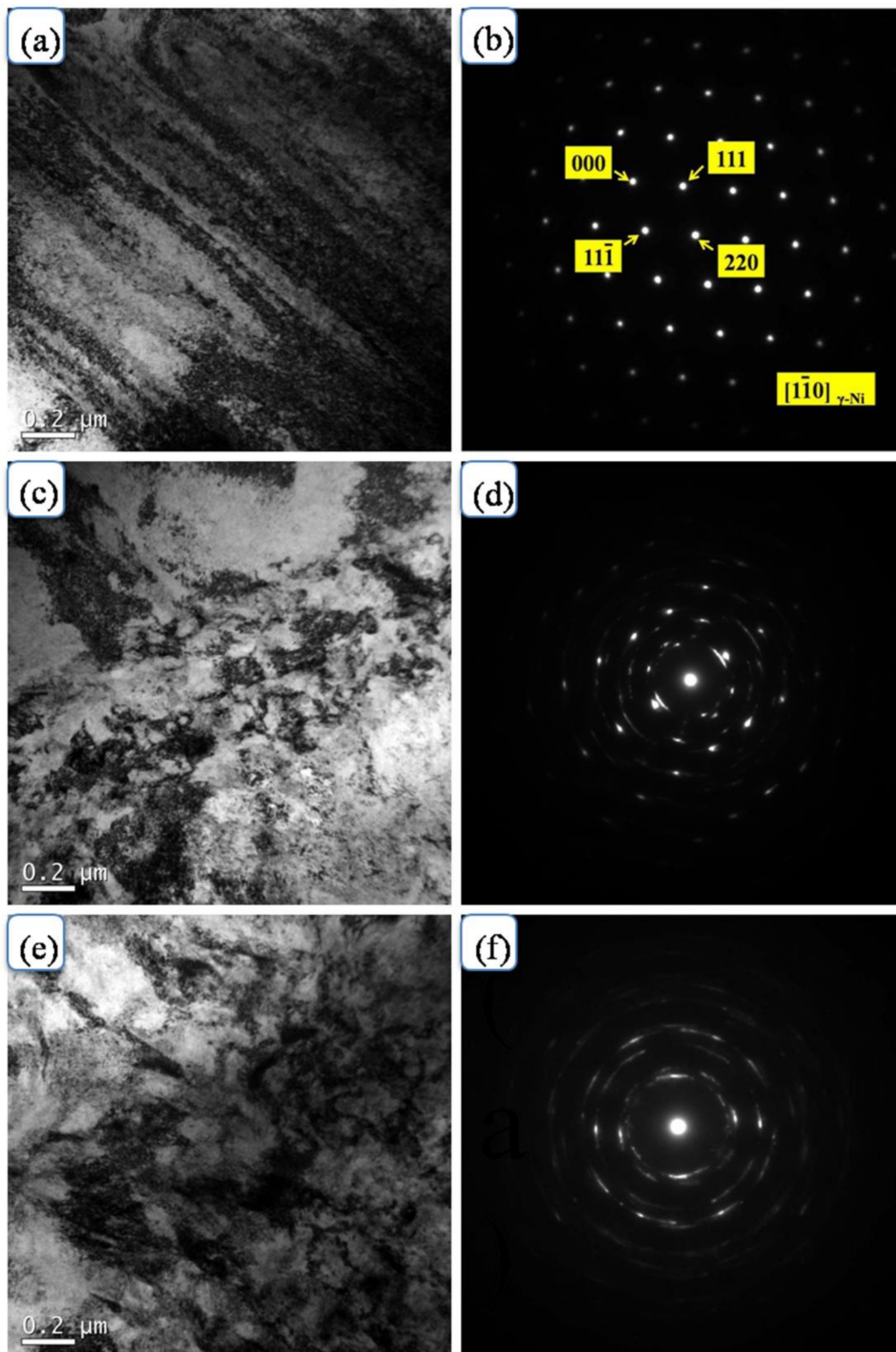
**Figure 9.** Cont.



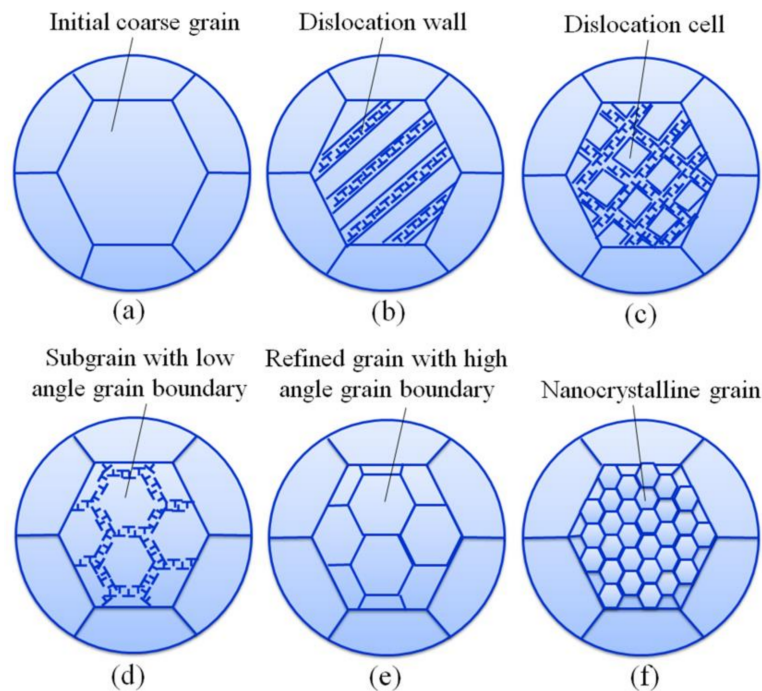
**Figure 9.** TEM micrographs of heat-treated Ni-Nb5 alloy: (a) Bright field image indicating  $\gamma$  matrix; (b) Diffraction pattern of (a); (c) Bright field image indicating  $\text{Ni}_3(\text{Al,Ti})$  phase; (d) Diffraction pattern of  $\text{Ni}_3(\text{Al,Ti})$  phase in (c).

Figure 10 shows TEM micrographs of the as-cast Ni-Nb5 alloy undergoing a compressive deformation degree by 60% at room temperature. It can be found from Figure 10 that the as-cast Ni-Nb5 alloy displays inhomogeneous plastic deformation, which is attributed to the fact that when the as-cast Ni-Nb5 alloy suffers from compression, the various deformation zones experience various plastic strains. As for the small plastic strain, it is observed that plenty of dislocations appear in the as-cast Ni-Nb5 alloy as shown in Figure 10a. This demonstrates that dislocation slip is responsible for plastic deformation of the as-cast Ni-Nb5 alloy. With increasing plastic strain, the grains are gradually refined as shown in Figure 10c. When the local region of the as-cast Ni-Nb5 alloy experiences a large plastic strain, nanocrystalline phases are able to be induced as illustrated in Figure 10e.

In our previous work, dislocation slip as well as deformation twinning was found to be the dominant plastic deformation mechanism of the as-cast Ni-Nb5 alloy at cryogenic temperatures [33,34]. However, in the present work, deformation twinning is not found to be the plastic deformation mechanism of the as-cast Ni-Nb5 alloy at room temperature. It is deduced that only dislocation slip is responsible for the plastic deformation of the as-cast Ni-Nb5 alloy at room temperature. According to the previous literature, the plastic deformation mechanisms of the as-cast Ni-Nb5 alloy at room temperature are generalized in Figure 11, where a typical grain is emphasized. Firstly, plastic deformation for dislocation slip results in the accumulation of dislocations. With the progression of plastic deformation, plenty of dislocations are induced as a result of a large plastic strain. Consequently, the dislocation walls are able to be formed under the interaction between dislocations. With the continuous increase of plastic strain, the dislocations are gradually accumulated such that the dislocation cells are capable of being formed eventually. Based on dislocation slip, subgrains with a low-angle grain boundary begin to appear. With increasing plastic strain, the low-angle grain boundary is converted to a high-angle grain boundary, which leads to the occurrence of the new fine grains eventually. The new fine grain is refined repeatedly and consequently nanocrystalline grains are generated [34].



**Figure 10.** TEM micrographs of as-cast Ni-Nb5 alloy undergoing compressive deformation degree by 60%: (a) Bright field image indicating high-density dislocations; (b) Diffraction pattern of (a); (c) Bright field image indicating refined grains; (d) Diffraction pattern of (c); (e) Bright field image indicating occurrence of nanocrystalline grains; (f) Diffraction pattern of (e).



**Figure 11.** Schematic diagram of the plastic deformation mechanism for the nanocrystallization of nickel-based alloy: (a) Initial coarse grain; (b) Dislocation walls formed as a result of dislocation slip; (c) Dislocation cells formed as a result of dislocation slip; (d) Subgrains with low angle grain boundary induced due to dislocation slip; (e) Grain refinement along with the occurrence of high angle grain boundary; (f) Nanocrystalline grain formed due to severe plastic deformation.

The plastic deformation mechanisms of heat-treated Ni-Nb5 alloy are different from those of as-cast Ni-Nb5 alloy because of the existence of  $\gamma'$  precipitates after heat treatment. The interaction between dislocations and  $\gamma'$  precipitates has an important influence on the plastic deformation mechanisms of nickel-based alloy. The plastic deformation mechanisms of Ni-based alloys are substantially influenced by deformation temperatures, where dislocation slip or dislocation climb plays a key role [18,19,35]. In addition, several novel deformation mechanisms are also found in a few nickel-based alloys containing  $\gamma'$  precipitates, which result from heat treatment. Cui et al. stated that the dominant deformation mechanisms of the M951G nickel-based superalloy at low creep temperatures deal with the isolated stacking faults shearing the  $\gamma'$  precipitates [35]. Unocic et al. stated that deformation microtwins are found during the creep deformation of nickel-based alloy, which is strengthened by a  $\gamma'$  precipitate [18]. Qiu et al. stated that the deformation mechanism of nickel-based alloy at room temperature is attributed to the fact that dislocations cut through secondary  $\gamma'$  precipitates and very fine  $\gamma'$  precipitates, where stacking faults are formed [19]. In the present work, it is concluded that  $\gamma'$  precipitates are able to become the obstacles to impede the movement of dislocations. This contributes to enhancing the yield strength of NiCuCrMoTiAlNb Ni-based alloy. However, with the progress of plastic deformation, the dislocations continuously pile up around the  $\gamma'$  precipitates and consequently micro-cracks are able to be induced, which shall lead to a decrease in the plasticity of NiCuCrMoTiAlNb nickel-based alloys.

#### 4. Conclusions

Three kinds of nickel-based alloys, whose compositions are based on Ni<sub>57-x</sub>Cu<sub>20</sub>Cr<sub>15</sub>Mo<sub>5</sub>Ti<sub>2</sub>Al<sub>1</sub>Nb<sub>x</sub> (wt %), where  $x$  represents 1, 3, and 5, respectively, were subjected to two-stage heat treatment. Furthermore, the influence of heat treatment on the microstructures and mechanical properties of NiCuCrMoTiAlNb nickel-based alloys was further investigated. The following conclusions are drawn.

(1) The as-cast NiCuCrMoTiAlNb nickel-based alloys are able to experience large plastic deformation at room temperature, where dislocation slip is the dominant plastic deformation mechanism. Based on the large plastic strain, nanocrystalline phases are able to be induced in the as-cast NiCuCrMoTiAlNb nickel-based alloys. The nanocrystallization process deals with the onset of dislocation walls, the occurrence of dislocation cells, the formation of subgrains with a low-angle grain boundary, and the generation of new grains with a high-angle grain boundary.

(2) In the case of heat-treated NiCuCrMoTiAlNb nickel-based alloy, plenty of  $\text{Ni}_3(\text{Al,Ti})$  precipitates ( $\gamma'$  phases) are distributed in the matrix and they are able to become the obstacles to impede the movement of dislocations, which is responsible for enhancing the yield strength of NiCuCrMoTiAlNb nickel-based alloys. Pileup of dislocations in the vicinity of  $\gamma'$  precipitates has an adverse effect on the plasticity of NiCuCrMoTiAlNb nickel-based alloy.

**Acknowledgments:** The work was financially supported by National Natural Science Foundation of China (Nos. 51475101 and 51305091).

**Author Contributions:** Shuyong Jiang wrote the manuscript; Dong Sun performed the XRD and SEM analysis; Yanqiu Zhang performed the OM and TEM analysis; Bingyao Yan performed the compression test and heat treatment experiment.

**Conflicts of Interest:** The authors declare no conflict of interest.

## References

1. Tao, J.; Chen, L.B.; Jiang, F.; Cai, H.P.; Sun, J. Microstructural evolution and mechanical properties of a nickel-based superalloy through long-term service. *Mater. Sci. Eng. A* **2016**, *656*, 184–189.
2. Prasad, K.; Sarkar, R.; Ghosal, P.; Kumar, V. Simultaneous creep-fatigue damage accumulation of forged turbine disc of In 718 superalloy. *Mater. Sci. Eng. A* **2013**, *572*, 1–7. [[CrossRef](#)]
3. Zhang, S.H.; Zhang, H.Y.; Cheng, M. Tensile deformation and fracture characteristics of delta-processed Inconel 718 alloy at elevated temperature. *Mater. Sci. Eng. A* **2011**, *528*, 6253–6258. [[CrossRef](#)]
4. Mostafaei, A.; Behnamian, Y.; Krimer, Y.L.; Stevens, E.L.; Luo, J.L.; Chmielus, M. Effect of solutionizing and aging on the microstructure and mechanical properties of powder bed binder jet printed nickel-based superalloy 625. *Mater. Des.* **2016**, *111*, 482–491. [[CrossRef](#)]
5. Sui, F.L.; Xua, L.X.; Chen, L.Q.; Liu, X.H. Processing map for hot working of Inconel 718 alloy. *J. Mater. Process. Technol.* **2011**, *211*, 433–440. [[CrossRef](#)]
6. Zhang, H.Y.; Zhang, S.H.; Cheng, M.; Li, Z.X. Deformation characteristics of  $\delta$  phase in the delta-processed Inconel 718 alloy. *Mater. Charact.* **2010**, *61*, 49–53. [[CrossRef](#)]
7. Lee, W.S.; Lin, C.F.; Chen, T.H.; Chen, H.W. Dynamic mechanical behaviour and dislocation substructure evolution of Inconel 718 over wide temperature range. *Mater. Sci. Eng. A* **2011**, *528*, 6279–6286. [[CrossRef](#)]
8. Thomas, A.; El-Wahabi, M.; Cabrera, J.M.; Prado, J.M. High temperature deformation of Inconel 718. *J. Mater. Process. Technol.* **2006**, *177*, 469–472. [[CrossRef](#)]
9. Lin, Y.C.; Li, K.K.; Li, H.B.; Chen, J.; Chen, X.M.; Wen, D.X. New constitutive model for high-temperature deformation behavior of Inconel 718 superalloy. *Mater. Des.* **2015**, *74*, 108–118. [[CrossRef](#)]
10. Qin, L.; Pei, Y.; Li, S.; Zhao, X.; Gong, S.; Xu, H. Effect of thermal stability of  $\gamma'$  phase on the recrystallization behaviors of Ni-based single crystal superalloys. *Mater. Des.* **2017**, *130*, 69–82. [[CrossRef](#)]
11. Marsh, C.; Depinoy, S.; Kaoumi, D. Effect of heat treatment on the temperature dependence of the fracture behavior of X-750 alloy. *Mater. Sci. Eng. A* **2016**, *677*, 474–484. [[CrossRef](#)]
12. Xie, J.; Tian, S.; Zhou, X.; Yu, X.; Wang, W. Influence of heat treatment regimes on microstructure and creep properties of FGH95 nickel base superalloy. *Mater. Sci. Eng. A* **2012**, *538*, 306–314. [[CrossRef](#)]
13. Lu, Y.L.; Liu, J.X.; Li, X.K.; Liang, J.P.; Li, Z.J.; Wu, G.Y.; Zhou, X.T. Hot deformation behavior of Hastelloy C276 superalloy. *Trans. Nonferrous Met. Soc. China* **2012**, *22*, s84–s88. [[CrossRef](#)]
14. Li, K.K.; Chen, M.S.; Lin, Y.C.; Yuan, W.Q. Microstructural evolution of an aged Ni-based superalloy under two-stage hot compression with different strain rates. *Mater. Des.* **2016**, *111*, 344–352. [[CrossRef](#)]
15. Lia, F.; Fua, R.; Yina, F.; Fenga, D.; Wang, H.Z.; Tiana, Z.L.; Dub, G.; Feng, Y. Impact of solution heat treatment on microstructure and creep behavior of a novel cast & wrought FGH4096 turbine disk alloy. *Mater. Sci. Eng. A* **2017**, *696*, 273–282.

16. He, D.G.; Lin, Y.C.; Chen, M.S.; Chen, J.; Wen, D.X.; Chen, X.M. Effect of pre-treatment on hot deformation behavior and processing map of an aged nickel-based superalloy. *J. Alloys Compd.* **2015**, *649*, 1075–1084. [[CrossRef](#)]
17. Azadia, M.; Maraboutb, A.; Safarloo, S.; Azadib, M.; Shariata, M.; Rizi, M.H. Effects of solutioning and ageing treatments on properties of Inconel-713C nickel-based superalloy under creep loading. *Mater. Sci. Eng. A* **2018**, *711*, 195–204. [[CrossRef](#)]
18. Unocic, R.R.; Zhou, N.; Kovarik, L.; Shen, C.; Wang, Y.; Mills, M.J. Dislocation decorrelation and relationship to deformation microtwins during creep of a  $\gamma'$  precipitate strengthened Ni-based superalloy. *Acta Mater.* **2011**, *59*, 7325–7339. [[CrossRef](#)]
19. Qiu, C.L.; Hua, X.; Mei, J.F.; Paul Andrews, P.; Voice, W. Influence of heat treatment on microstructure and tensile behavior of a hot isostatically pressed nickel-based superalloy. *J. Alloys Compd.* **2013**, *578*, 454–464. [[CrossRef](#)]
20. Özgür Özgün; Yılmaz, R.; Gülsoy, H.Ö.; Fındık, F. The effect of aging treatment on the fracture toughness and impact strength of injection molded Ni-625 superalloy parts. *Mater. Charact.* **2015**, *108*, 8–15.
21. Pröbstle, M.; Neumeier, S.; Feldner, P.; Rettig, R.; Helmer, H.E.; Singer, R.F.; Göken, M. Improved creep strength of nickel-base superalloys by optimized  $\gamma/\gamma'$  partitioning behavior of solid solution strengthening elements. *Mater. Sci. Eng. A* **2016**, *676*, 411–420. [[CrossRef](#)]
22. Cao, G.H.; Sun, T.Y.; Wang, C.H.; Li, X.; Liu, M.; Zhang, Z.X. Investigations of  $\gamma'$ ,  $\gamma''$  and  $\delta$  precipitates in heat-treated inconel 718 alloy fabricated by selective laser melting. *Mater. Charact.* **2018**, *136*, 398–406. [[CrossRef](#)]
23. You, X.; Tan, Y.; Zhao, L.; You, Q.; Wang, Y.; Ye, F. Effect of solution heat treatment on microstructure and electrochemical behavior of electron beam smelted inconel 718 superalloy. *J. Alloys Compd.* **2018**, *741*, 792–803. [[CrossRef](#)]
24. Lin, Y.C.; Li, L.; He, D.G.; Chen, M.S.; Liu, G.Q. Effects of pre-treatments on mechanical properties and fracture mechanism of a nickel-based superalloy. *Mater. Sci. Eng. A* **2016**, *679*, 401–409. [[CrossRef](#)]
25. Souza, G.R.X.D.; Gabriel, S.B.; Dille, J.; Santos, D.S.D.; Almeida, L.H.D. Work hardening and aging contribution on the mechanical properties of x-750 nickel-based superalloy. *Mater. Sci. Eng. A* **2013**, *564*, 102–106. [[CrossRef](#)]
26. Li, C.; Yuan, Z.; Fan, Y.; He, S.; Xuan, W.; Li, X. Microstructure and mechanical properties of a Ni-based superalloy after heat treatment in a steady magnetic field. *J. Mater. Process. Technol.* **2017**, *246*, 176–184. [[CrossRef](#)]
27. Rahimi, S.; King, M.; Dumont, C. Stress relaxation behaviour in IN718 nickel based superalloy during ageing heat treatments. *Mater. Sci. Eng. A* **2017**, *708*, 563–573. [[CrossRef](#)]
28. Mignanelli, P.M.; Jones, N.G.; Perkins, K.M.; Hardy, M.C.; Stone, H.J. Microstructural evolution of a delta containing nickel-base superalloy during heat treatment and isothermal forging. *Mater. Sci. Eng. A* **2015**, *621*, 265–271. [[CrossRef](#)]
29. Wen, D.X.; Lin, Y.C.; Chen, J.; Deng, J.; Chen, X.M.; Zhang, J.L.; He, M. Effects of initial aging time on processing map and microstructures of a nickel-based superalloy. *Mater. Sci. Eng. A* **2015**, *620*, 319–332.
30. Zhang, P.; Yuan, Y.; Yan, J.B.; Wang, J.C.; Song, X.L.; Yang, G.X. Morphological evolution of  $\gamma'$  precipitates in superalloy M4706 during thermal aging. *Mater. Lett.* **2018**, *211*, 107–109. [[CrossRef](#)]
31. Ha, J.W.; Seong, B.S.; Jeong, H.W.; Choi, Y.S.; Kang, N. Effects of the aging temperature and stress relaxation conditions on  $\gamma'$  precipitation in inconel x-750. *J. Nucl. Mater.* **2015**, *457*, 362–368. [[CrossRef](#)]
32. Zhang, Y.; Liu, L.; Huang, T.; Li, Y.; Jie, Z.; Zhang, J. Investigation on remelting solution heat treatment for nickel-based single crystal superalloys. *Scr. Mater.* **2017**, *136*, 74–77. [[CrossRef](#)]
33. Jiang, S.Y.; Sun, D.; Zhang, Y.Q.; Zhu, X.M.; Wang, M.; Zhao, C.Z. Plastic deformation mechanisms of NiCuCrMoTiAlNb Ni-based alloys at cryogenic temperature. *Mater. Sci. Eng. A* **2016**, *664*, 135–145. [[CrossRef](#)]
34. Jiang, S.Y.; Zhang, Y.Q.; Zhu, X.M.; Sun, D.; Wang, M.; Zhao, C.Z. Physical mechanisms of nanocrystallization of a novel Ni-based alloy under uniaxial compression at cryogenic temperature. *Mater. Charact.* **2016**, *116*, 18–23. [[CrossRef](#)]
35. Cui, L.; Yu, J.; Liu, J.; Jin, T.; Sun, X. The creep deformation mechanisms of a newly designed nickel-base superalloy. *Mater. Sci. Eng. A* **2018**, *710*, 309–317. [[CrossRef](#)]

